Robust Joint Position Feedback Control of Robot Manipulators

Tesheng Hsiao[1]
Department of Electrical
and Computer Engineering,
National Chiao Tung University,
1001 Ta Hsueh Road,
Hsinchu, 30010, Taiwan
e-mail: tshsiao@cn.nctu.edu.tw

Mao-Chiao Weng
Institute of Electrical and Control Engineering,
National Chiao Tung University,
1001 Ta Hsueh Road,
Hsinchu, 30010, Taiwan
e-mail: mchiao.weng@gmail.com

Most manipulator motion controllers require joint velocity feedback. Whenever joint velocities are not measurable, they are estimated from the joint positions. However, velocity estimates tend to be inaccurate under low-speed motion or low sensor resolution conditions. Moreover, velocity estimators may either be susceptible to model uncertainties or introduce additional dynamics (e.g., phase lag) to the control loop. Consequently, direct substitution of velocity estimates into the controller results in the deterioration of the control performance and robustness margin. Therefore, this paper proposes a robust position-feedback motion controller which gets rid of the problems of uncompensated dynamics and model uncertainties introduced by velocity estimators. Furthermore, a globally asymptotically stable system, which is robust with respective to model parameter variations, is guaranteed. Theoretical analysis and experimental verifications are carried out. The results demonstrate that the proposed controller is robust and outperforms the conventional computed torque plus proportional integral differential (PID) controller.
[DOI: 10.1115/1.4023669]

Keywords: manipulators, robots, position feedback, motion control, robust control

1 Introduction

Motion control of robot manipulators has been an active research topic for the past two decades [1,2]. It concerns accurate and robust tracking of the desired trajectories in the task space or the joint space under the adverse influence of model uncertainties and limited feedback information. Model uncertainties are inevitable and may come from various sources. For example, it is found to be difficult to accurately model friction forces; the payload of the manipulator may change from time to time. On the contrary, joint velocity feedback is required by most modern control laws; some control algorithms even require joint acceleration feedback. However, the measurements of joint velocities and accelerations are either contaminated by substantial noise or not available in many robotic systems due to cost and weight reduction. In this paper, we investigate the robust trajectory tracking problem, with respect to model parameter variations, and the feedback information is restricted to joint positions only. The proposed controller guarantees global robust stability and zero asymptotic tracking errors. Then experiments are conducted to verify the robust performance.

We briefly review the previous work in the area of manipulator motion control. Because the manipulator's dynamics is nonlinear, it is a common practice to implement feedback linearization, also known as the computed torque approach, as the first step of controller design [3]. Then linear control laws, such as the proportional-derivative (PD) controller [4], are applied to the feedback-linearized system. The simplification and modification of the computed torque controller for highly geared manipulators were investigated in Refs. [5,6]. Similarly, a proportional-integral (PI)-type controller was implemented in the joint velocity inner loop with reference signals coming from the kinematic outer loop [7]. Since cancellation of the nonlinear dynamics is imperfect in the presence of model uncertainties, more advanced controllers have been explored to enhance robustness [8,9].

For example, adaptive control and sliding mode control have been extensively studied in the area of manipulator trajectory tracking. Craig et al. [10] proposed an adaptive control algorithm with guaranteed global asymptotic stability. However, the assumptions that the estimated inertia matrix remains positive definite all the time and the joint accelerations are available may not always be satisfied [11]. Spong and Ortega [12] removed the first assumption in their adaptive control law while Slotine and Li [13,14] proposed an adaptive controller without joint acceleration feedback. Besides, adaptive algorithms for the simultaneous motion and force tracking control of manipulators have been investigated in Ref. [15].

Early work on the sliding mode control of manipulators can be found in Ref. [16]. Subsequent modifications eliminated the need to calculate the inverse inertia matrix [17,18]. Recent research has addressed alleviating the chattering phenomenon and achieving the sliding surface in finite time. Zhihong et al. [19] designed a robust multi-input multi-output sliding mode controller which drives the output tracking error to zero in finite time in the presence of model uncertainties. Moura et al. [20] proposed a frequency-shaped sliding mode controller with good tracking ability and reduced chattering. Yu and Chen [21] proposed a sliding mode controller with sequentially operated sliding surfaces. The upper bound of the traveling time for each sliding surface was computable and the robustness was enhanced.

All aforementioned controllers require joint velocity feedback; some also require acceleration feedback. However in many industrial robot manipulators, the measurements of joint velocities are either unavailable or contaminated by substantial noise. Therefore, the need for velocity estimation arises. The backward difference of positions is commonly used as a velocity estimate because of its simple form, however, it tends to be inaccurate under low-speed motion or low sensor resolution conditions. Besides, backward difference estimation suffers from high-frequency measurement noise. Filtering techniques [22,23] are also widely used to estimate velocities; however the additional phase lag introduced by the filter may be harmful to the closed-loop system. The undesirable vibration of the manipulators caused by replacing the velocity feedback terms with filtered positions has been reported in Ref. [24]. Velocity estimators based on robot dynamic models [25], kinematic relations along with acceleration measurements [26,27], and numerical integration [28] have been studied. Although these velocity estimators have been shown to be effective in velocity estimation, their cooperation with controllers in closed-loop systems requires further investigation.

On the contrary, a variety of observer-based controllers with only joint position feedback were proposed, including sliding

[1]Corresponding author.

Contributed by the Dynamic Systems Division of ASME for publication in the Journal of Dynamic Systems, Measurement, and Control. Manuscript received May 25, 2010; final manuscript received December 11, 2012; published online March 28, 2013. Editor: J. Karl Hedrick.

mode observers [29], nonlinear high-gain observers [30], and linear observers with adaptive controllers [31,32] or with variable structure controllers [33]. Due to the nonlinearity of the manipulator and model uncertainties, these controllers can only guarantee local exponential stability or uniform ultimate boundedness of the closed-loop system.

In this paper, we propose a robust controller with only joint position feedback. Unlike the aforementioned methods, the proposed controller implicitly incorporates the velocity estimator; thus eliminating the problem of uncompensated dynamics and model uncertainties introduced by the velocity estimator or observer. Consequently, a globally asymptotically stable system, which is robust with respect to model parameter variations, is guaranteed. A theoretical analysis and experimental verifications will be carried out in subsequent sections.

This paper is organized as follows: Sec. 2 introduces the dynamic model of the manipulator. Section 3 presents the design procedure of the proposed controller and proves its robust stability. Experimental results are presented in Sec. 4. Section 5 concludes this paper.

2 Dynamic Model of the Manipulator

The dynamic equation of an n-joint manipulator is given as follows:

$$\mathbf{M}(\mathbf{q}(t))\ddot{\mathbf{q}}(t) + \mathbf{C}(\mathbf{q}(t), \dot{\mathbf{q}}(t))\dot{\mathbf{q}}(t) + \mathbf{G}(\mathbf{q}(t)) + \mathbf{B}\dot{\mathbf{q}}(t) + \mathbf{F}(\dot{\mathbf{q}}(t)) = \boldsymbol{\tau}(t) \quad (1)$$

where $\mathbf{q}(t)$, $\dot{\mathbf{q}}(t)$, and $\ddot{\mathbf{q}}(t) \in \mathbb{R}^n$ are the vectors of the joint positions, velocities, and accelerations at time t, respectively. Here, $\mathbf{M}(\mathbf{q}(t))$, $\mathbf{C}(\mathbf{q}(t), \dot{\mathbf{q}}(t))$, amd $\mathbf{B} \in \mathbb{R}^{n\times n}$ denote the inertia matrix, the Coriolis and the centrifugal matrix, and the viscous friction coefficient matrix, respectively. In Eq. (1), $\mathbf{G}(\mathbf{q}(t))$, $\mathbf{F}(\dot{\mathbf{q}}(t))$, and $\boldsymbol{\tau}(t) \in \mathbb{R}^n$ are the gravitational torque vector, the Coulomb friction vector, and the control torque vector, respectively. For clarity, we will drop the notational dependence of all variables on t as long as it leads to no confusion.

Note that the inertia matrix $\mathbf{M}(\mathbf{q})$ is positive definite for all $\mathbf{q}$ [34]. If we decompose $\mathbf{M}(\mathbf{q})$ as a sum of a constant positive definite matrix $\mathbf{M}_0$ and a time varying matrix $\mathbf{M}_1(\mathbf{q})$, i.e., $\mathbf{M}(\mathbf{q}) = \mathbf{M}_0 + \mathbf{M}_1(\mathbf{q})$, then Eq. (1) can be rearranged as follows:

$$\mathbf{M}_0\ddot{\mathbf{q}} + \mathbf{B}\dot{\mathbf{q}} = \boldsymbol{\tau} - \mathbf{h}(\mathbf{q}, \dot{\mathbf{q}}, \ddot{\mathbf{q}}) \quad (2)$$

where

$$\mathbf{h}(\mathbf{q}, \dot{\mathbf{q}}, \ddot{\mathbf{q}}) = \mathbf{M}_1(\mathbf{q})\ddot{\mathbf{q}} + \mathbf{C}(\mathbf{q}, \dot{\mathbf{q}})\dot{\mathbf{q}} + \mathbf{G}(\mathbf{q}) + \mathbf{F}(\dot{\mathbf{q}})$$

In the remainder of this paper, we will use $\mathbf{h}(t)$ or $\mathbf{h}$, instead of $\mathbf{h}(\mathbf{q}, \dot{\mathbf{q}}, \ddot{\mathbf{q}})$ to simplify the notation.

To take into account model parameter variations, we assume that

$$\mathbf{M}_0^* = \mathbf{M}_0 + \Delta\mathbf{M}_0, \quad \mathbf{M}_1^*(\mathbf{q}) = \mathbf{M}_1(\mathbf{q}) + \Delta\mathbf{M}_1(\mathbf{q}), \quad \mathbf{C}^*(\mathbf{q}, \dot{\mathbf{q}}) = \mathbf{C}(\mathbf{q}, \dot{\mathbf{q}}) + \Delta\mathbf{C}(\mathbf{q}, \dot{\mathbf{q}})$$
$$\mathbf{G}^*(\mathbf{q}) = \mathbf{G}(\mathbf{q}) + \Delta\mathbf{G}(\mathbf{q}) \quad \mathbf{B}^* = \mathbf{B} + \Delta\mathbf{B}, \quad \mathbf{F}^*(\dot{\mathbf{q}}) = \mathbf{F}(\dot{\mathbf{q}}) + \Delta\mathbf{F}(\dot{\mathbf{q}})$$

where an asterisk in the superscript denotes the nominal value. The notations with a Δ on the left side denote uncertain matrices or vectors. We made the following assumption about their upper bounds.

Assumption 1. *The manipulator is assumed to be equipped with revolute joints only and there exist known positive constants* Δ_{M_0}, Δ_{M_1}, Δ_C, Δ_G, Δ_B, *and* Δ_F *such that for all* $\mathbf{q}, \dot{\mathbf{q}} \in \mathbb{R}^n$, *we have*

$$\|\Delta\mathbf{M}_0\| \le \Delta_{M_0}, \quad \|\Delta\mathbf{M}_1(\mathbf{q})\| \le \Delta_{M_1}, \quad \|\Delta\mathbf{C}(\mathbf{q}, \dot{\mathbf{q}})\| \le \Delta_C\|\dot{\mathbf{q}}\|$$
$$\|\Delta\mathbf{G}(\mathbf{q})\| \le \Delta_G, \quad \|\Delta\mathbf{B}\| \le \Delta_B, \quad \|\Delta\mathbf{F}(\dot{\mathbf{q}})\| \le \Delta_F$$

The notation $\|\cdot\|$ *denotes the Euclidian norm of a vector, or the induced 2-norm of a matrix.*

Remark. If the manipulator is equipped with revolute joints only, the Coriolis and centrifugal matrix satisfies [34]: (i) $\mathbf{C}^*(\mathbf{q}, \mathbf{x})\mathbf{y} = \mathbf{C}^*(\mathbf{q}, \mathbf{y})\mathbf{x}$, (ii) $\mathbf{C}^*(\mathbf{q}, \mathbf{x}+\mathbf{y})\mathbf{z} = \mathbf{C}^*(\mathbf{q}, \mathbf{x})\mathbf{z} + \mathbf{C}^*(\mathbf{q}, \mathbf{y})\mathbf{z}$, and (iii) $\exists\, k_{C1} > 0$ such that $\|\mathbf{C}^*(\mathbf{q}, \mathbf{x})\mathbf{y}\| \le k_{C1}\|\mathbf{x}\|\|\mathbf{y}\|$ for any $\mathbf{q}, \mathbf{x}, \mathbf{y}, \mathbf{z} \in \mathbb{R}^n$. These properties are useful for determining a tighter upper bound of the residual term (17). However, a more conservative upper bound can also be found without applying these properties. Therefore the assumption of revolute joints is not restrictive and the proposed control law is still applicable to manipulators with prismatic joints.

3 Controller Design and Robust Stability Analysis

We suppose that the task of the manipulator has been defined such that the manipulator must follow a desired joint position $\mathbf{q}_d(t)$, velocity $\dot{\mathbf{q}}_d(t)$, and acceleration $\ddot{\mathbf{q}}_d(t)$. The tracking position error, velocity error, and acceleration error are defined, respectively, as

$$\tilde{\mathbf{q}} = \mathbf{q} - \mathbf{q}_d, \quad \dot{\tilde{\mathbf{q}}} = \dot{\mathbf{q}} - \dot{\mathbf{q}}_d, \quad \ddot{\tilde{\mathbf{q}}} = \ddot{\mathbf{q}} - \ddot{\mathbf{q}}_d$$

The proposed control law consists of the following three terms:

$$\boldsymbol{\tau}(t) = \boldsymbol{\tau}_{\text{Lin}}(t) + \boldsymbol{\tau}_{\text{LC}}(t) + \boldsymbol{\tau}_{\text{NC}}(t) \quad (3)$$

where $\boldsymbol{\tau}_{\text{Lin}}$ is the linearization torque, which uses nominal models and the desired trajectory to cancel the manipulator's nominal nonlinear part, $\boldsymbol{\tau}_{\text{LC}}$ is the linear control torque, which stabilizes the manipulator's linear part (i.e., the left hand side of Eq. (2)) and reduces tracking errors, and $\boldsymbol{\tau}_{\text{NC}}$ is the nonlinear control torque, which guarantees global robust asymptotic stability of the closed-loop system. Since we are designing a position feedback controller, each term of Eq. (3) should depend on $\mathbf{q}$, but not on $\dot{\mathbf{q}}$ or $\ddot{\mathbf{q}}$.

3.1 Linearization Torque.

The linearization torque $\boldsymbol{\tau}_{\text{Lin}}$ is used to cancel the nominal nonlinear part of the manipulator. Namely

$$\boldsymbol{\tau}_{\text{Lin}} = \mathbf{M}_1^*(\mathbf{q})\ddot{\mathbf{q}}_d + \mathbf{C}^*(\mathbf{q}, \dot{\mathbf{q}}_d)\dot{\mathbf{q}}_d + \mathbf{G}^*(\mathbf{q}) + \mathbf{F}^*(\dot{\mathbf{q}}_d) \quad (4)$$

Cancellation of the nonlinear part of the manipulator is imperfect in the presence of model uncertainties, which must be compensated by additional control efforts.

3.2 Linear Control Torque.

The linear control torque $\boldsymbol{\tau}_{\text{LC}}$ is designed to stabilize the linear part of the manipulator and to reduce the tracking error. The reasons for applying linear control laws are: (i) it has been reported that the dynamics of the manipulator with high gear ratios can be approximated by a linear system [2,34], (ii) if the linearization torque works perfectly, then the manipulator behaves like an linear time-invariant system: $\mathbf{M}_0\ddot{\mathbf{q}} + \mathbf{B}\dot{\mathbf{q}} = \boldsymbol{\tau}_{\text{LC}}$ (see Eq. (2)), (iii) in spite of the imperfect cancellation of the nonlinear dynamics, small discrepancies between $\boldsymbol{\tau}_{\text{Lin}}$ and $\mathbf{h}$ are tolerable by a robust linear controller, and (iv) there exist many

well-established design methods and software tools to facilitate the task of linear controller design.

Since only the joint positions are measurable, the linear controller under consideration must follow an output feedback law. However, it is generally true that an output feedback controller can be decomposed into a state feedback controller and a (reduced order) observer [35,36]. Moreover, it has been shown that a static state feedback controller is able to achieve the same performance as that which can be achieved by a dynamic state feedback controller [37]. Therefore, it suffices to design a static state feedback controller to accomplish the control objectives provided that all state variables are available.

Observers are incorporated into the control loop whenever some state variables are unavailable. Introducing stable observers into the loop does not ruin the stability established by the state feedback controller; however, the robustness margin is no longer guaranteed [38]. This is because the observer's dynamics is not taken into account in the design of the state feedback controller. To solve this problem, we propose an output-feedback controller design procedure which consists of two steps: first, a state feedback control law is derived based on the "augmented system" as if all state variables were available. Second, the state feedback control law is converted into an output feedback control law. During the conversion, neither observers nor any other dynamic systems are introduced; hence, the closed-loop system remains unaltered.

Step I: State Feedback Control Law. The manipulator (2) is augmented with an $n \times n$ transfer matrix $\mathbf{\Lambda}(s)$ cascaded in the input side. The augmented system is shown inside the dashed-line box of Fig. 1. We are going to find a state feedback control law $\mathbf{v}$ such that the augmented system is stabilized and the tracking error is reduced. First, let

$$\mathbf{\Lambda}(s) = \text{diag}\left(\frac{1}{s+\lambda_1}, \cdots, \frac{1}{s+\lambda_n}\right) \tag{5}$$

where diag(…) denotes a (block) diagonal matrix with diagonal elements enclosed by the parentheses. Here, λ_i, $i = 1,\ldots,n$ are design parameters to be determined later. Suppose that $\mathbf{\Lambda}(s)$ has the following state space representation:

$$\begin{aligned} \dot{\boldsymbol{\eta}} &= \mathbf{A}_\eta \boldsymbol{\eta} + \mathbf{v} \\ \boldsymbol{\tau}_{\text{LC}} &= \boldsymbol{\eta} \end{aligned} \tag{6}$$

where $\mathbf{A}_\eta = \text{diag}(-\lambda_1, -\lambda_2, \ldots, -\lambda_n)$. Next, we define the desired linear torque as

$$\boldsymbol{\tau}_d = \mathbf{M}_0^* \ddot{\mathbf{q}}_d + \mathbf{B}^* \dot{\mathbf{q}}_d \tag{7}$$

In other words, we assume that the desired trajectory is generated by applying $\boldsymbol{\tau}_d$ to the nominal linear part of the manipulator. Accordingly the desired input to the augmented system is defined as $\hat{\mathbf{v}}_d(s) = \mathbf{\Lambda}^{-1}(s)\hat{\boldsymbol{\tau}}_d(s)$, where the notation $\hat{\bullet}(s)$ refers to the Laplace transform of $\bullet(t)$. Therefore

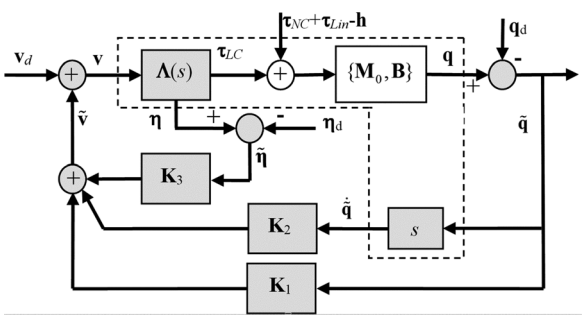

Fig. 1 The augmented system and the linear controller

$$\begin{aligned} \dot{\boldsymbol{\eta}}_d &= \mathbf{A}_\eta \boldsymbol{\eta}_d + \mathbf{v}_d \\ \boldsymbol{\tau}_d &= \boldsymbol{\eta}_d \end{aligned} \tag{8}$$

We would like to find a state feedback control law such that the augmented system (i.e., Eqs. (2) and (6)) "behaves like" the desired augmented system (i.e., Eqs. (7) and (8)). To do this, let $\tilde{\boldsymbol{\eta}} = \boldsymbol{\eta} - \boldsymbol{\eta}_d$ and $\tilde{\mathbf{v}} = \mathbf{v} - \mathbf{v}_d$; then from Eqs. (6) and (8) we obtain

$$\dot{\tilde{\boldsymbol{\eta}}} = \mathbf{A}_\eta \tilde{\boldsymbol{\eta}} + \tilde{\mathbf{v}} \tag{9}$$

On the contrary, we can derive from Eqs. (2), (3), and (7) that

$$\tilde{\boldsymbol{\eta}} = \boldsymbol{\tau}_{\text{LC}} - \boldsymbol{\tau}_d = \mathbf{M}_0^* \ddot{\tilde{\mathbf{q}}} + \mathbf{B}^* \dot{\tilde{\mathbf{q}}} - (\boldsymbol{\tau}_{\text{NC}} + \boldsymbol{\tau}_{\text{Lin}} - \mathbf{h}) - \Delta\boldsymbol{\tau}_d \tag{10}$$

where $\Delta\boldsymbol{\tau}_d = \Delta\mathbf{M}_0\ddot{\mathbf{q}} + \Delta\mathbf{B}\dot{\mathbf{q}}$. If we define $\tilde{\mathbf{x}} = [\,\tilde{\mathbf{q}}^T \quad \dot{\tilde{\mathbf{q}}}^T \quad \tilde{\boldsymbol{\eta}}^T\,]^T$, then rearranging Eqs. (9) and (10) yields

$$\dot{\tilde{\mathbf{x}}} = \mathbf{A}_a \tilde{\mathbf{x}} + \mathbf{B}_{a1}\tilde{\mathbf{v}} + \mathbf{B}_{a2}(\boldsymbol{\tau}_{\text{NC}} + \boldsymbol{\tau}_{\text{Lin}} - \mathbf{h} + \Delta\boldsymbol{\tau}_d) \tag{11}$$

where

$$\mathbf{A}_a = \begin{bmatrix} \mathbf{0} & \mathbf{I} & \mathbf{0} \\ \mathbf{0} & -(\mathbf{M}_0^*)^{-1}\mathbf{B}^* & (\mathbf{M}_0^*)^{-1} \\ \mathbf{0} & \mathbf{0} & \mathbf{A}_\eta \end{bmatrix}, \quad \mathbf{B}_{a1} = \begin{bmatrix} \mathbf{0} \\ \mathbf{0} \\ \mathbf{I} \end{bmatrix}, \quad \mathbf{B}_{a2} = \begin{bmatrix} \mathbf{0} \\ (\mathbf{M}_0^*)^{-1} \\ \mathbf{0} \end{bmatrix}$$

Suppose that the nominal linear part of the manipulator is controllable from $\boldsymbol{\tau}_{\text{LC}}$; then it is easy to show that $(\mathbf{A}_a, \mathbf{B}_{a1})$ is also controllable by the Popov–Belevitch–Hautus test. Thus, we can find a state feedback law $\tilde{\mathbf{v}}(t) = -\mathbf{K}\tilde{\mathbf{x}}(t)$, such that $\mathbf{A}_a - \mathbf{B}_{a1}\mathbf{K}$ is Hurwitz. Note that $\mathbf{h}$ and $\Delta\boldsymbol{\tau}_d$ in Eq. (11) cannot be treated as external disturbances since they are functions of the state. However, the residual $\boldsymbol{\tau}_{\text{Lin}} - \mathbf{h} + \Delta\boldsymbol{\tau}_d$ will be small if the nominal model is accurate enough. In such a case, we may wonder whether a robust linear controller along with the linearization torque is able to achieve a satisfactory performance. Nevertheless, it is expected that the performance will deteriorate severely when the residual becomes large. The experimental results in Sec. 4 verify this point of view.

Step II: Output Feedback Control Law. The state feedback law of Step I can be expressed as

$$\tilde{\mathbf{v}}(t) = -\mathbf{K}_1\tilde{\mathbf{q}}(t) - \mathbf{K}_2\dot{\tilde{\mathbf{q}}}(t) - \mathbf{K}_3\tilde{\boldsymbol{\eta}}(t) \tag{12}$$

where $\mathbf{K} = [\mathbf{K}_1 \ \mathbf{K}_2 \ \mathbf{K}_3]$ and $\mathbf{K}_i \in \mathbb{R}^{n\times n}$ for $i = 1,2,3$. Because $\hat{\tilde{\boldsymbol{\eta}}}(s) = \hat{\boldsymbol{\tau}}_{\text{LC}}(s) - \hat{\boldsymbol{\tau}}_d(s) = \mathbf{\Lambda}(s)\hat{\tilde{\mathbf{v}}}(s)$, taking Laplace transforms on both sides of Eq. (12) leads to

$$\hat{\tilde{\mathbf{v}}}(s) = -\left(\mathbf{K}_1\hat{\tilde{\mathbf{q}}}(s) + \mathbf{K}_2\hat{\dot{\tilde{\mathbf{q}}}}(s) + \mathbf{K}_3\hat{\tilde{\boldsymbol{\eta}}}(s)\right) = \mathbf{\Lambda}^{-1}(s)\hat{\tilde{\boldsymbol{\eta}}}(s)$$

Hence, $\hat{\tilde{\boldsymbol{\eta}}}(s) = -\left[\mathbf{\Lambda}^{-1}(s) + \mathbf{K}_3\right]^{-1}[\mathbf{K}_1 + s\mathbf{K}_2]\hat{\tilde{\mathbf{q}}}(s)$, and the output feedback control law is

$$\hat{\boldsymbol{\tau}}_{\text{LC}}(s) = \hat{\boldsymbol{\tau}}_d(s) + \hat{\tilde{\boldsymbol{\eta}}}(s) = \hat{\boldsymbol{\tau}}_d(s) - \left[\mathbf{\Lambda}^{-1}(s) + \mathbf{K}_3\right]^{-1}[\mathbf{K}_1 + s\mathbf{K}_2]\hat{\tilde{\mathbf{q}}}(s) \tag{13}$$

Upon designing the state feedback controller, $\mathbf{\Lambda}(s)$ is regarded as a part of the plant, i.e., the augmented system. We choose state feedback gains $\mathbf{K}_1$, $\mathbf{K}_2$, and $\mathbf{K}_3$ to stabilize the augmented system and to establish a desired robustness margin. In Fig. 1, the blocks inside the dashed-line box constitute the augmented plant while the blocks outside the dashed-line box belong to the state feedback controller. When the state feedback controller is converted into the output feedback controller, $\mathbf{\Lambda}(s)$ becomes a part of the controller. Namely, the output feedback controller comprises all shaded blocks in Fig. 1. It is clear from Fig. 1 that no additional

dynamic systems (e.g., observers, filters, or velocity estimators) are added to the loop during the conversion; hence, the closed-loop systems of the state feedback controller (with respect to the augmented plant) and the output feedback controller (with respect to the original plant) are identical. Consequently, the output feedback controller preserves the stability and robustness properties of the state feedback controller. Note that the state feedback controller (12) must accomplish the control objectives. If the state feedback controller cannot achieve the goal, neither can the output feedback controller (13). This is because these two controllers end up with the same closed-loop system.

Remarks.

(1) Since $\mathbf{\Lambda}(s)$ has a relative degree of 1, $\tilde{\mathbf{C}}_{\mathrm{LC}}(s) \triangleq [\mathbf{\Lambda}^{-1}(s) + \mathbf{K}_3]^{-1}[\mathbf{K}_1 + s\mathbf{K}_2]$ is proper and realizable. Therefore, Eq. (13) is indeed an output feedback controller, which is the difference between $\boldsymbol{\tau}_d$ and the filtered position error $\tilde{\mathbf{C}}_{\mathrm{LC}}(s)\hat{\tilde{\mathbf{q}}}(s)$.

(2) Here, $\tilde{\mathbf{C}}_{\mathrm{LC}}(s)$ has the form of the "filtered PD controller;" however, its design procedure is more delicate than that of the conventional PD controller, which directly replaces the velocities with their estimates. As will be illustrated in the rest of this subsection, the coefficients of $\mathbf{\Lambda}(s)$ can be regarded as weightings of some cost function and the feedback gain $\mathbf{K}$ is the optimal solution that minimizes the cost function.

Robustness of the state feedback control system can be achieved by various modern control methods such as pole placement, linear quadratic regulation (LQR) control [39], H_∞ state feedback control [40], and mixed H_2/H_∞ state feedback control [41], etc. In this paper, we use the LQR method because of its salient robustness property. It is well known that the LQR controller has an infinite gain margin, at least 60 deg phase margin, and guaranteed stability in the event of 50% gain reduction [39]. The LQR controller (of the augmented system) minimizes the following cost function:

$$J = \int_0^\infty \tilde{\mathbf{x}}^T(t)\mathbf{Q}\tilde{\mathbf{x}}(t) + \tilde{\mathbf{v}}^T(t)\mathbf{R}\tilde{\mathbf{v}}(t)dt$$

The weighting matrix $\mathbf{Q}$ is positive semidefinite and $\mathbf{R}$ is positive definite. The LQR controller is

$$\tilde{\mathbf{v}} = -\mathbf{K}\tilde{\mathbf{x}} = -\mathbf{R}^{-1}\mathbf{B}_{a1}^T\mathbf{P}\tilde{\mathbf{x}} \tag{14}$$

where $\mathbf{P}$ is the symmetric positive definite solution to the Riccati equation

$$\mathbf{A}_a^T\mathbf{P} + \mathbf{P}\mathbf{A}_a - \mathbf{P}\mathbf{B}_{a1}\mathbf{R}^{-1}\mathbf{B}_{a1}^T\mathbf{P} + \mathbf{Q} = \mathbf{0} \tag{15}$$

If we choose $\mathbf{R} = \mathrm{diag}(r_1,\ldots,r_n)$ and $\mathbf{Q} = \mathrm{diag}(\mathbf{Q}_1,\mathbf{Q}_2)$, where $r_i > 0$ for all i, $\mathbf{Q}_1 \in \mathbb{R}^{2n\times 2n}$ is positive semi- definite, and $\mathbf{Q}_2 \in \mathbb{R}^{n\times n}$ is positive definite, then according to Eq. (9), the cost function becomes

$$J = \int_0^\infty \left(\begin{bmatrix} \tilde{\mathbf{q}}^T, \dot{\tilde{\mathbf{q}}}^T \end{bmatrix} \mathbf{Q}_1 \begin{bmatrix} \tilde{\mathbf{q}} \\ \dot{\tilde{\mathbf{q}}} \end{bmatrix} + \tilde{\boldsymbol{\eta}}^T\mathbf{Q}_2\tilde{\boldsymbol{\eta}} + \sum_{i=1}^{n} r_i\left(\dot{\tilde{\eta}}_i + \lambda_i\tilde{\eta}_i\right)^2 \right) dt \tag{16}$$

where $\tilde{\eta}_i$ denotes the ith element of the vector $\tilde{\boldsymbol{\eta}} = \boldsymbol{\tau}_{\mathrm{LC}} - \boldsymbol{\tau}_d$. From Eq. (16) we can see that λ_i can be regarded as the weighting of $\tilde{\eta}_i$, while the first derivative of $\tilde{\eta}_i$ is weighted by r_i. Therefore, the larger r_i is, the smoother the ith linear control torque is. On the contrary, if $r_i \to 0$ for all i, then the cost function approaches the LQR cost function of the original plant (with states $\tilde{\mathbf{q}}$ and $\dot{\tilde{\mathbf{q}}}$, input $\tilde{\boldsymbol{\eta}}$, and weighting matrices $\mathbf{Q}_1$ and $\mathbf{Q}_2$). In such a case, the effects of $\mathbf{\Lambda}(s)$ diminish.

Upon designing the linear control torque, the effects of the residual $\boldsymbol{\tau}_{\mathrm{Lin}} - \mathbf{h} + \Delta\boldsymbol{\tau}_d$ are not explicitly taken into account. Although the residual $\boldsymbol{\tau}_{\mathrm{Lin}} - \mathbf{h} + \Delta\boldsymbol{\tau}_d$ contains model uncertainties and cannot be known exactly, the upper bound of its size can be found as follows:

$$\begin{aligned}\|\boldsymbol{\tau}_{\mathrm{Lin}} - \mathbf{h} + \Delta\boldsymbol{\tau}_d\| &= \left\|-\mathbf{M}_1^*(\mathbf{q})\ddot{\tilde{\mathbf{q}}} + (\Delta\mathbf{M}_1(\mathbf{q}) + \Delta\mathbf{M}_0)\ddot{\mathbf{q}} + \Delta\mathbf{B}\dot{\mathbf{q}} + \mathbf{C}^*(\mathbf{q},\dot{\mathbf{q}}_d)\dot{\mathbf{q}}_d - \mathbf{C}^*(\mathbf{q},\dot{\mathbf{q}})\dot{\mathbf{q}} + \Delta\mathbf{C}(\mathbf{q},\dot{\mathbf{q}})\dot{\mathbf{q}} + \Delta\mathbf{G}(\mathbf{q}) + \Delta\mathbf{F}(\dot{\mathbf{q}}) + \mathbf{F}^*(\dot{\mathbf{q}}_d) - \mathbf{F}^*(\dot{\mathbf{q}})\right\| \\ &\le \left\|\mathbf{M}_1^*(\mathbf{q})\right\| \cdot \left\|\ddot{\tilde{\mathbf{q}}}\right\| + (\Delta_{M_1} + \Delta_{M_0})\left(\left\|\ddot{\tilde{\mathbf{q}}}\right\| + \left\|\ddot{\mathbf{q}}_d\right\|\right) + \Delta_B\left(\left\|\dot{\tilde{\mathbf{q}}}\right\| + \left\|\dot{\mathbf{q}}_d\right\|\right) + (k_{C1} + \Delta_C)\left\|\dot{\tilde{\mathbf{q}}}\right\| \cdot \left(\left\|\dot{\tilde{\mathbf{q}}}\right\| + 2\left\|\dot{\mathbf{q}}_d\right\|\right) \\ &\quad + \Delta_C\left\|\dot{\mathbf{q}}_d\right\|^2 + \Delta_G + \Delta_F + 2\|\mathbf{F}^*\|\end{aligned} \tag{17}$$

Suppose that there exist $U_1(t), U_2(t) \in \mathbb{R}$ such that

$$\left\|\dot{\tilde{\mathbf{q}}}(t)\right\| \le U_1(t), \quad \left\|\ddot{\tilde{\mathbf{q}}}(t)\right\| \le U_2(t), \quad \text{for all} \quad t \ge 0 \tag{18}$$

Then

$$\begin{aligned}\|\boldsymbol{\tau}_{\mathrm{Lin}} - \mathbf{h} + \Delta\boldsymbol{\tau}_d\| &\le \left\|\mathbf{M}_1^*(\mathbf{q})\right\| \cdot U_2 + (\Delta_{M_1} + \Delta_{M_0})(U_2 + \|\ddot{\mathbf{q}}_d\|) \\ &\quad + \Delta_B(U_1 + \|\dot{\mathbf{q}}_d\|) + (k_{C1} + \Delta_C)U_1 \cdot (U_1 + 2\|\dot{\mathbf{q}}_d\|) \\ &\quad + \Delta_C\|\dot{\mathbf{q}}_d\|^2 + \Delta_G + \Delta_F + 2\|\mathbf{F}^*\| \triangleq \bar{\delta}(t)\end{aligned}$$

Section 3.4 will illustrate how to find $U_1(t)$ and $U_2(t)$. The upper bound of the residual will be used in the design of the nonlinear control torque.

3.3 Nonlinear Control Torque. The nonlinear control torque is designed to guarantee the robust asymptotic stability of the closed-loop system. We also want to keep the total control torque as small as possible in order to not saturate the actuator. To achieve this goal, we first consider the following Lyapunov function candidate:

$$V_1(\tilde{\mathbf{x}}) = \tilde{\mathbf{x}}^T\mathbf{P}\tilde{\mathbf{x}}$$

where $\mathbf{P} = \mathbf{P}^T > 0$ is the solution to Eq. (15). Let $\mathbf{P} = [\mathbf{P}_1\ \mathbf{P}_2\ \mathbf{P}_3]$ and $\mathbf{P}_i \in \mathbb{R}^{3n\times n}$, for $i = 1,2,3$. By using Eqs. (11), (14), and (15), the time derivative of V_1 is

$$\begin{aligned}\dot{V}_1 &= \dot{\tilde{\mathbf{x}}}^T\mathbf{P}\tilde{\mathbf{x}} + \tilde{\mathbf{x}}^T\mathbf{P}\dot{\tilde{\mathbf{x}}} \\ &= \tilde{\mathbf{x}}^T\left(\mathbf{A}_a^T\mathbf{P} + \mathbf{P}\mathbf{A}_a - 2\mathbf{P}\mathbf{B}_{a1}\mathbf{R}^{-1}\mathbf{B}_{a1}^T\mathbf{P}\right)\tilde{\mathbf{x}} \\ &\quad + 2\tilde{\mathbf{x}}^T\mathbf{P}\mathbf{B}_{a2}(\boldsymbol{\tau}_{\mathrm{NC}} + \boldsymbol{\tau}_{\mathrm{Lin}} - \mathbf{h} + \Delta\boldsymbol{\tau}_d) \\ &= -\tilde{\mathbf{x}}^T\left(\mathbf{Q} + \mathbf{P}\mathbf{B}_{a1}\mathbf{R}^{-1}\mathbf{B}_{a1}^T\mathbf{P}\right)\tilde{\mathbf{x}} \\ &\quad + 2\tilde{\mathbf{x}}^T\mathbf{P}_2(\mathbf{M}_0^*)^{-1}(\boldsymbol{\tau}_{\mathrm{NC}} + \boldsymbol{\tau}_{\mathrm{Lin}} - \mathbf{h} + \Delta\boldsymbol{\tau}_d)\end{aligned}$$

The LQR controller guarantees that the first term of the last equation is negative for all nonzero $\tilde{\mathbf{x}}$; thus $\boldsymbol{\tau}_{\mathrm{NC}}$ will be designed to counteract the 2nd term $\tilde{\mathbf{x}}^T\mathbf{P}_2(\mathbf{M}_0^*)^{-1}(\boldsymbol{\tau}_{\mathrm{Lin}} - \mathbf{h} + \Delta\boldsymbol{\tau}_d)$, such that $\dot{V}_1$ is negative definite. If all elements of $\tilde{\mathbf{x}}$ are measurable, the robust stability can be ensured by techniques such as saturation-type control [42]. To overcome the problem of the lack of velocity feedback, we apply a strictly positive real (SPR) system to generate the nonlinear control torque.

Let $\mathbf{H}(s)$ be an $n \times n$ SPR system with input $\mathbf{z}(t) \triangleq (\mathbf{M}_0^*)^{-T}\mathbf{P}_2^T\tilde{\mathbf{x}}(t)$ and output $\boldsymbol{\phi}(t)$. Then, the nonlinear control torque is chosen to be

$$\boldsymbol{\tau}_{\mathrm{NC}}(t) = -\alpha(t)\boldsymbol{\phi}(t) \tag{19}$$

where the time-varying gain $\alpha(t)$ is to be determined.

At first glance, it seems that the implementation of $\boldsymbol{\tau}_{\mathrm{NC}}$ still requires the full state information $\tilde{\mathbf{x}}$. However, the difficulty can be bypassed by carefully manipulating the equations. Let $(\mathbf{M}_0^*)^{-T}\mathbf{P}_2^T = [\mathbf{E}_1 \quad \mathbf{E}_2 \quad \mathbf{E}_3]$, where $\mathbf{E}_i \in \mathbb{R}^{n\times n}$ for $i = 1,2,3$. Then

$$\begin{aligned}\hat{\boldsymbol{\phi}}(s) &= \mathbf{H}(s)\hat{\mathbf{z}}(s)\\ &= \mathbf{H}(s)\left(\mathbf{E}_1\hat{\tilde{\mathbf{q}}}(s) + \mathbf{E}_2 s\hat{\tilde{\mathbf{q}}}(s) + \mathbf{E}_3\hat{\tilde{\boldsymbol{\eta}}}(s)\right)\\ &= (\mathbf{H}(s)\mathbf{E}_1 + s\mathbf{H}(s)\mathbf{E}_2)\hat{\tilde{\mathbf{q}}}(s) + \mathbf{H}(s)\mathbf{E}_3\hat{\tilde{\boldsymbol{\eta}}}(s)\end{aligned} \tag{20}$$

If $\mathbf{H}(s)$ is the SPR with a relative degree of 1, then $\boldsymbol{\phi}$ can be obtained by filtering $\tilde{\mathbf{q}}$ and $\tilde{\boldsymbol{\eta}}$ through two proper filters $\mathbf{H}(s)\mathbf{E}_1 + s\mathbf{H}(s)\mathbf{E}_2$ and $\mathbf{H}(s)\mathbf{E}_3$, respectively. Furthermore, suppose that $\mathbf{H}(s)$ has the following minimal realization:

$$\begin{aligned}\dot{\boldsymbol{\zeta}}(t) &= \mathbf{A}_\zeta\boldsymbol{\zeta}(t) + \mathbf{B}_\zeta\mathbf{z}(t)\\ \boldsymbol{\phi}(t) &= \mathbf{C}_\zeta\boldsymbol{\zeta}(t)\end{aligned}$$

By using the Kalman–Yakubovich–Popov theorem [43], if all eigenvalues of $\mathbf{A}_\zeta$ lie in the left half plane of $\mathrm{Re}(s) < -\gamma$ for some positive constant γ, then there exists an $n \times n$ symmetric positive definite matrix $\boldsymbol{\Gamma}$ and a matrix $\mathbf{Q}_\zeta$ such that

$$\begin{aligned}\mathbf{A}_\zeta^T\boldsymbol{\Gamma} + \boldsymbol{\Gamma}\mathbf{A}_\zeta &= -\mathbf{Q}_\zeta\mathbf{Q}_\zeta^T - 2\gamma\boldsymbol{\Gamma}\\ \boldsymbol{\Gamma}\mathbf{B}_\zeta &= \mathbf{C}_\zeta^T\end{aligned}$$

Let α^* and K_α be two positive constants selected by the designer. Define $\tilde{\alpha}(t) = \alpha(t) - \alpha^*$ and choose the following Lyapunov function:

$$V(\tilde{\mathbf{x}}(t), \boldsymbol{\zeta}(t), \tilde{\alpha}(t)) = V_1(\tilde{\mathbf{x}}(t)) + \alpha^*\boldsymbol{\zeta}^T(t)\boldsymbol{\Gamma}\boldsymbol{\zeta}(t) + K_\alpha\tilde{\alpha}^2(t)$$

For clarity, we use the notation $V(t)$ instead of $V(\tilde{\mathbf{x}}(t), \boldsymbol{\zeta}(t), \tilde{\alpha}(t))$ if it leads to no confusion. Clearly, $V(t) \geq 0$ for all $t \geq 0$ and $V(t) = 0$ if and only if $\tilde{\mathbf{x}}(t) = \mathbf{0}$, $\boldsymbol{\zeta}(t) = \mathbf{0}$, and $\tilde{\alpha}(t) = 0$. The time derivative of $V(t)$ is

$$\begin{aligned}\dot{V} &= \dot{V}_1 + \alpha^*\dot{\boldsymbol{\zeta}}^T\boldsymbol{\Gamma}\boldsymbol{\zeta} + \alpha^*\boldsymbol{\zeta}^T\boldsymbol{\Gamma}\dot{\boldsymbol{\zeta}} + K_\alpha\frac{d}{dt}(\tilde{\alpha}^2)\\ &= -\tilde{\mathbf{x}}^T\bar{\mathbf{Q}}\tilde{\mathbf{x}} + \alpha^*\boldsymbol{\zeta}^T\left(\mathbf{A}_\zeta^T\boldsymbol{\Gamma} + \boldsymbol{\Gamma}\mathbf{A}_\zeta\right)\boldsymbol{\zeta} + 2\tilde{\mathbf{x}}^T\mathbf{P}_2(\mathbf{M}_0^*)^{-1}(-\alpha\mathbf{C}_\zeta\boldsymbol{\zeta} + \boldsymbol{\tau}_{\mathrm{Lin}} - \mathbf{h} + \Delta\boldsymbol{\tau}_d) + 2\alpha^*\mathbf{z}^T\mathbf{B}_\zeta^T\boldsymbol{\Gamma}\boldsymbol{\zeta} + K_\alpha\frac{d}{dt}(\tilde{\alpha}^2)\\ &= -\tilde{\mathbf{x}}^T\bar{\mathbf{Q}}\tilde{\mathbf{x}} - \alpha^*\boldsymbol{\zeta}^T\left(\mathbf{Q}_\zeta\mathbf{Q}_\zeta^T + 2\gamma\boldsymbol{\Gamma}\right)\boldsymbol{\zeta} + 2\tilde{\mathbf{x}}^T\mathbf{P}_2(\mathbf{M}_0^*)^{-1}(-\alpha\mathbf{C}_\zeta\boldsymbol{\zeta} + \boldsymbol{\tau}_{\mathrm{Lin}} - \mathbf{h} + \Delta\boldsymbol{\tau}_d) + 2\alpha^*\tilde{\mathbf{x}}^T\mathbf{P}_2(\mathbf{M}_0^*)^{-1}\mathbf{C}_\zeta\boldsymbol{\zeta} + K_\alpha\frac{d}{dt}(\tilde{\alpha}^2)\\ &= -\tilde{\mathbf{x}}^T\bar{\mathbf{Q}}\tilde{\mathbf{x}} - \alpha^*\boldsymbol{\zeta}^T\left(\mathbf{Q}_\zeta\mathbf{Q}_\zeta^T + 2\gamma\boldsymbol{\Gamma}\right)\boldsymbol{\zeta} + 2\tilde{\mathbf{x}}^T\mathbf{P}_2(\mathbf{M}_0^*)^{-1}(\boldsymbol{\tau}_{\mathrm{Lin}} - \mathbf{h} + \Delta\boldsymbol{\tau}_d) - 2\tilde{\alpha}\tilde{\mathbf{x}}^T\mathbf{P}_2(\mathbf{M}_0^*)^{-1}\mathbf{C}_\zeta\boldsymbol{\zeta} + K_\alpha\frac{d}{dt}(\tilde{\alpha}^2)\end{aligned}$$

where $\bar{\mathbf{Q}} = \mathbf{Q} + \mathbf{P}\mathbf{B}_{a1}\mathbf{R}^{-1}\mathbf{B}_{a1}^T\mathbf{P}$ and $\mathbf{Q}_\zeta\mathbf{Q}_\zeta^T + 2\gamma\boldsymbol{\Gamma}$ are positive definite.

If Eq. (18) holds, then

$$\|\tilde{\mathbf{x}}\| = \sqrt{\|\tilde{\mathbf{q}}\|^2 + \|\dot{\tilde{\mathbf{q}}}\|^2 + \|\tilde{\boldsymbol{\eta}}\|^2} \leq \sqrt{\|\tilde{\mathbf{q}}\|^2 + U_1^2 + \|\tilde{\boldsymbol{\eta}}\|^2} \triangleq U_x(t)$$

In addition, we have

$$\tilde{\mathbf{x}}^T\mathbf{P}_2(\mathbf{M}_0^*)^{-1}(\boldsymbol{\tau}_{\mathrm{Lin}} - \mathbf{h} + \Delta\boldsymbol{\tau}_d) \leq U_x\|\mathbf{P}_2(\mathbf{M}_0^*)^{-1}\|\bar{\delta}$$

and

$$\tilde{\alpha}\tilde{\mathbf{x}}^T\mathbf{P}_2(\mathbf{M}_0^*)^{-1}\mathbf{C}_\zeta\boldsymbol{\zeta} \leq U_x|\tilde{\alpha}|\|\mathbf{P}_2(\mathbf{M}_0^*)^{-1}\|\|\mathbf{C}_\zeta\boldsymbol{\zeta}\|$$

If we define $|\tilde{\alpha}_1| = \tilde{\alpha}^2$, then $d/dt(\tilde{\alpha}^2) = d/dt|\tilde{\alpha}_1| = \dot{\tilde{\alpha}}_1\mathrm{sgn}(\tilde{\alpha}_1)$, where $\mathrm{sgn}(\bullet)$ is the sign function. Let

$$\begin{aligned}\dot{\tilde{\alpha}}_1 &= \frac{-2U_x\|\mathbf{P}_2(\mathbf{M}_0^*)^{-1}\|\left(\bar{\delta} + \|\mathbf{C}_\zeta\boldsymbol{\zeta}\|\sqrt{|\tilde{\alpha}_1|}\right)\mathrm{sgn}(\tilde{\alpha}_1)}{K_\alpha} - \frac{\tilde{\alpha}_1}{K_\alpha}\\ \alpha &= \alpha^* - \sqrt{|\tilde{\alpha}_1|}\end{aligned} \tag{21}$$

Clearly, $\dot{\tilde{\alpha}}_1 > 0$ if and only if $\tilde{\alpha}_1 < 0$. Therefore $\tilde{\alpha}_1$ will converge to zero and, consequently, α will converge to α^*. Substituting Eq. (21) into $\dot{V}$ yields

$$\begin{aligned}\dot{V} &= -\tilde{\mathbf{x}}^T\bar{\mathbf{Q}}\tilde{\mathbf{x}} - \alpha^*\boldsymbol{\zeta}^T\left(\mathbf{Q}_\zeta\mathbf{Q}_\zeta^T + 2\gamma\boldsymbol{\Gamma}\right)\boldsymbol{\zeta}\\ &\quad + \left[2\tilde{\mathbf{x}}^T\mathbf{P}_2(\mathbf{M}_0^*)^{-1}(\boldsymbol{\tau}_{\mathrm{Lin}} - \mathbf{h} + \Delta\boldsymbol{\tau}_d) - 2U_x\|\mathbf{P}_2(\mathbf{M}_0^*)^{-1}\|\bar{\delta}\right]\\ &\quad + \left[-2\tilde{\alpha}\tilde{\mathbf{x}}^T\mathbf{P}_2(\mathbf{M}_0^*)^{-1}\mathbf{C}_\zeta\boldsymbol{\zeta} - 2U_x|\tilde{\alpha}|\|\mathbf{P}_2(\mathbf{M}_0^*)^{-1}\|\|\mathbf{C}_\zeta\boldsymbol{\zeta}\|\right] - \tilde{\alpha}^2\\ &\leq -\tilde{\mathbf{x}}^T\bar{\mathbf{Q}}\tilde{\mathbf{x}} - \alpha^*\boldsymbol{\zeta}^T\left(\mathbf{Q}_\zeta\mathbf{Q}_\zeta^T + 2\gamma\boldsymbol{\Gamma}\right)\boldsymbol{\zeta} - \tilde{\alpha}^2\end{aligned} \tag{22}$$

Therefore, $\dot{V}$ is negative definite for all initial conditions, which implies that the closed-loop system is globally asymptotically stable and $\tilde{\mathbf{x}}\to 0$, $\alpha(t) \to \alpha^*$ as $t \to \infty$, i.e., the tracking error asymptotically approaches zero and the nonlinear control torque gain $\alpha(t)$ approaches a steady state gain α^*, which is selected by the designer.

Remarks.

(1) The design parameters of the nonlinear control torque include $\mathbf{H}(s)$, K_α, and α^*. There are no restrictions on selecting these parameters except that α^* and K_α are positive, and $\mathbf{H}(s)$ is the SPR with a relative degree of 1. Therefore, the design procedure can be easily accomplished. For example, we can choose $\mathbf{H}(s) = \mathrm{diag}(\gamma_1/(s+\gamma_1), \ldots, \gamma_n/(s+\gamma_n))$, where $\gamma_i > 0$, $i = 1,\ldots,n$, is larger than the bandwidth of $q_{id}(t)$, which is the ith element of $\mathbf{q}_d$. In addition, note that K_α is canceled out in $\dot{V}$ and thus has no influence on the stability of the closed-loop system. However a larger K_α makes the differential Eq. (21) less stiff and hence improves the numerical accuracy in implementing Eq. (21). On the contrary, α^* is the steady state gain of the nonlinear control torque. A small gain prevents the nonlinear control torque from saturating the actuator, but results in the slow convergence of the Lyapunov function (see Eq. (22)).

(2) The proposed controller (3) can be interpreted as follows: $\boldsymbol{\tau}_{\mathrm{Lin}}$ is the feedback linearization term, $\boldsymbol{\tau}_{\mathrm{LC}}$ is the "filtered PD" term, and $\boldsymbol{\tau}_{\mathrm{NC}}$ is the "filtered state feedback" term with time-varying gain. Although filters are introduced in calculating $\boldsymbol{\tau}_{\mathrm{LC}}$ and $\boldsymbol{\tau}_{\mathrm{NC}}$, the dynamics of these filters are explicitly compensated in the controller design and, therefore, robust stability is guaranteed. Moreover, the filtering processes are accomplished by first order systems for each joint (i.e., $\boldsymbol{\Lambda}(s)$ and $\mathbf{H}(s)$). Hence, the complexity of the proposed

controller (3) is moderate. The experiments in Sec. 4 demonstrate that Eq. (3) can easily be implemented on modern microcontroller chips.

3.4 Upper Bounds of the Tracking Errors. Upper bounds of the velocity and acceleration tracking errors, i.e., $U_1(t)$ and $U_2(t)$ in Eq. (18), are required in calculating the nonlinear control torque gain (21). This subsection illustrates how to find these upper bounds based on the position tracking error $\tilde{\mathbf{q}}$.

Let $G(s) = a/(s+a)$, $a > 0$, and define $\hat{p}_i(s) = G(s)\hat{\dot{\tilde{q}}}_i(s) = (sG(s))\hat{\tilde{q}}_i(s)$, $i = 1,\ldots,n$, i.e., p_i is the filtered velocity tracking error of the ith joint, which can be obtained from $\tilde{q}_i$ because $sG(s)$ is proper. Let $G_d(z) = (1-\bar{a})/(1-\bar{a}z^{-1})$ be the discrete-time approximation to $G(s)$ [44] with the impulse response $g_k = (1-\bar{a})\bar{a}^k$, $k \in \mathbb{Z}^+$, where $\bar{a} = e^{-aT_s} < 1$ and T_s is the sampling time. If $p_i(0) = 0$, then

$$|p_i(kT_s)| = |g_k * \dot{\tilde{q}}_i(kT_s)| \approx \left|\sum_{m=0}^{k} g_{k-m}\dot{\tilde{q}}_i(mT_s)\right| \le \left(\max_{0\le m\le k}|\dot{\tilde{q}}_i(mT_s)|\right)\sum_{m=0}^{k}|g_{k-m}| \le \|\dot{\tilde{q}}_i\|_{k\infty}\|g\|_1 \quad (23)$$

where "*" denotes the discrete-time convolution, $||\bullet||_1$ is the l_1-norm, and $||\bullet||_{k\infty}$ is the l_∞-norm of $\bullet$ truncated up to time kT_s [45], i.e., $||\dot{\tilde{q}}_i||_{k\infty} \triangleq \max_{0\le m\le k}|\dot{\tilde{q}}_i(mT_s)|$. Note that the last inequality of Eq. (23) also holds for all $p_i(mT_s)$, $0 \le m \le k$; hence, we have $||p_i||_{k\infty} \le ||\dot{\tilde{q}}_i||_{k\infty}||g||_1$.

On the contrary, let δ be the discrete-time impulse signal. Then

$$\|\dot{\tilde{q}}_i\|_{k\infty} - \|p_i\|_{k\infty} \le \|\dot{\tilde{q}}_i - p_i\|_{k\infty} = \|(\delta - g) * \dot{\tilde{q}}_i\|_{k\infty} \le \|\delta - g\|_1\|\dot{\tilde{q}}_i\|_{k\infty}$$

where $||\delta - g||_1 = |1-g_0| + \sum_{k=1}^{\infty}|g_k| = 2\bar{a}$. If $\bar{a} < 1/2$, or equivalently, $a > \ln 2/T_s$, then

$$|\dot{\tilde{q}}_i(kT_s)| \le \|\dot{\tilde{q}}_i\|_{k\infty} \le \frac{1}{c}\|p_i\|_{k\infty} \quad (24)$$

where $c = 1 - ||\delta - g||_1 = 1 - 2\bar{a}$. Equation (24) provides an upper bound to the velocity tracking error at $t = kT_s$. For small T_s, we can assume that $|\dot{\tilde{q}}_i(t)| \le (1/c)||p_i||_{k\infty}$ for $kT_s \le t < k+1)T_s$.

Similarly, we define $\hat{p}'_i(s) = G(s)\hat{\ddot{\tilde{q}}}_i(s)$ and $\hat{\bar{p}}_i(s) = G(s)\hat{p}'_i(s) = G^2(s)\hat{\dddot{\tilde{q}}}_i(s) = s^2G^2(s)\hat{\tilde{q}}_i(s)$. Then, following the same arguments, we have

$$|\ddot{\tilde{q}}_i(kT_s)| \le \frac{1}{c}\|p'_i\|_{k\infty} \le \frac{1}{c^2}\|\bar{p}_i\|_{k\infty} \quad (25)$$

Given the inequalities (24) and (25), the upper bounds U_1 and U_2 in Eq. (18) become

$$U_1(t) = \frac{1}{c}\sqrt{\sum_{i=1}^{n}\|p_i\|_{k\infty}^2} \quad \text{and} \quad U_2(t) = \frac{1}{c^2}\sqrt{\sum_{i=1}^{n}\|\bar{p}_i\|_{k\infty}^2} \quad \text{for} \quad kT_s \le t < (k+1)T_s$$

Remark. The robust asymptotic stability of the proposed control system does not rely on precise estimates of joint velocities; instead, only the upper bounds of the velocity and acceleration tracking errors are required. Therefore a simple filter $G(s)$ suffices for this purpose. There is no need to implement complicated (nonlinear) state observers to estimate the velocities, nor to use filtered positions as imprecise substitutes for the velocities. In addition, the upper bounds in Eqs. (24) and (25) are immune to model uncertainties; hence, they do not degrade the robustness margin of the control system.

4 Experiments

4.1 Experimental Setting. A two-joint planar manipulator was set up for experimental verifications. The schema and the photograph of the manipulator are shown in the left and right sides of Fig. 2, respectively.

Each link of the manipulator is driven by a dc motor with an optical encoder mounted on the shaft. The controller is implemented on a DSP chip (TMS320F28335) and the sampling time is 0.01 s. The dynamics of the dc motors and the manipulator can be lumped together as follows [2,34]:

$$\begin{bmatrix}\theta_1+\theta_2+2\theta_3\cos q_2 & \theta_2+\theta_3\cos q_2\\ \theta_7+\theta_8\cos q_2 & \theta_7+\theta_9\end{bmatrix}\begin{bmatrix}\ddot{q}_1\\ \ddot{q}_2\end{bmatrix} + \begin{bmatrix}-\theta_3\dot{q}_2\sin q_2 & -\theta_3(\dot{q}_1+\dot{q}_2)\sin q_2\\ \theta_8\dot{q}_1\sin q_2 & 0\end{bmatrix}\begin{bmatrix}\dot{q}_1\\ \dot{q}_2\end{bmatrix} + \begin{bmatrix}\theta_4\cos q_1 + \frac{g}{l_1}\theta_3\cos(q_1+q_2)\\ \frac{g}{l_1}\theta_8\cos(q_1+q_2)\end{bmatrix} + \begin{bmatrix}\theta_5\dot{q}_1+\theta_6\,\mathrm{sgn}\,\dot{q}_1\\ \theta_{10}\dot{q}_2+\theta_{11}\,\mathrm{sgn}\,(\dot{q}_2)\end{bmatrix} = \begin{bmatrix}u_1\\ u_2\end{bmatrix}$$

where the control inputs u_1 and u_2 are armature voltages of the dc motors in the range of ± 24 V. Here, θ_i, $i = 1,2,\ldots,11$, are model parameters, as explained in Table 1. Their values are determined by the system identification techniques [46] and are also given in Table 1. The SI unit system is adopted for all physical quantities. Table 2 lists the nomenclature for the model parameters.

4.2 Experimental Results. The desired trajectory is specified as

$$q_{1d}(t) = -\frac{\pi}{2} + \frac{\pi}{4}(1-e^{-2t^3}) + \frac{\pi}{9}(1-e^{-2t^3})\sin(4t)$$
$$q_{2d}(t) = \frac{\pi}{3}(1-e^{-2t^3}) + \frac{\pi}{6}(1-e^{-2t^3})\sin(3t)$$

The corresponding path of the tip of the 2nd link in the task space is shown in Fig. 3. This trajectory consists of both a steady-state periodic motion (sinusoidal term) and a transient part (exponential term); therefore, it is suitable for exploring the abilities and limitations of motion controllers. We implement the proposed controller (3) and other types of controllers to compare their performance; however, a comprehensive experimental evaluation of all controllers is beyond the scope of this paper. Instead, we choose the computed torque plus PID controller for comparison. The reasons are twofold: (i) the computed torque plus PID

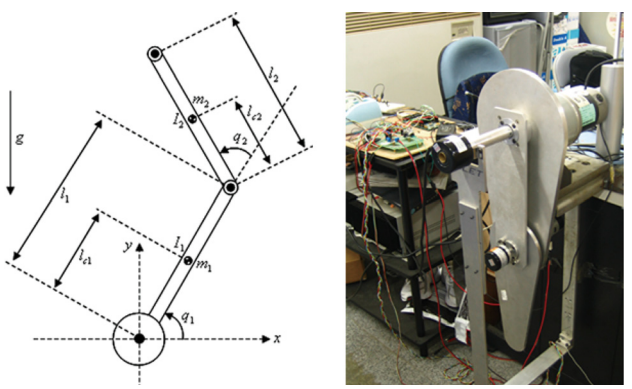

Fig. 2 Schema of the two-joint planar manipulator (left). Photograph of the manipulator (right).

Table 1 Model parameters and their nominal values

$\theta_1 = \left[(I_1 + m_1 l_{c1}^2 + m_2 l_1^2)\frac{1}{r_1^2} + J_1\right]\frac{1}{k_1}$	0.3339		$\theta_2 = (I_2 + m_2 l_{c2}^2)\frac{1}{r_1^2 k_1}$	0.0048	
$\theta_3 = m_2 l_1 l_{c2}\frac{1}{r_1^2 k_1}$	0.0054	$\theta_4 = (m_1 l_{c1} + m_2 l_1) g \frac{1}{r_1^2}\frac{1}{k_1}$	2.1450	$\theta_5 = b_1\frac{1}{k_1}$	2.8219
$\theta_6 = f_{c1}\frac{1}{r_1^2}\frac{1}{k_1}$	1.5177	$\theta_7 = (I_2 + m_2 l_{c2}^2)\frac{1}{r_2^2 k_2}$	0.0240	$\theta_8 = m_2 l_1 l_{c2}\frac{1}{r_2^2 k_2}$	0.0280
$\theta_9 = J_2\frac{1}{r_2^2 k_2}$	0.00002	$\theta_{10} = b_2\frac{1}{k_2}$	1.2211	$\theta_{11} = f_{c2}\frac{1}{r_2^2}\frac{1}{k_2}$	1.6282

Table 2 Nomenclature of the model parameters

I_1, (I_2)	Moment of inertia of the 1st (2nd) link
m_1, (m_2)	Mass of the 1st (2nd) joint
l_1, (l_2)	Length of the 1st (2nd) joint
l_{c1}, (l_{c2})	Distance from the joint to the CG of the 1st (2nd) link
J_1, (J_2)	Inertia of the motor's rotor of the 1st (2nd) joint
r_1, (r_2)	Gear ratio of the 1st (2nd) joint
k_1, (k_2)	Lumped constants of motors in the 1st (2nd) joint
f_{c1}, (f_{c2})	Coulomb friction coefficients of the 1st (2nd) joint
b_1, (b_2)	Combined viscous friction coefficients
g	Gravity acceleration

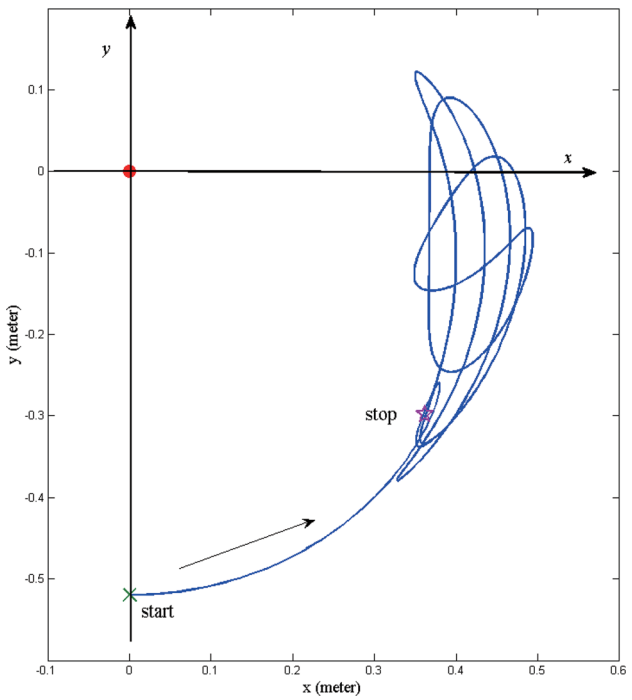

Fig. 3 The desired path of the tip of the 2nd link in the task space

controller has been extensively studied and practically implemented. Its properties are well known, and (ii) it is relatively easy to tune the PID gains, such that the adverse impact caused by the velocity estimator can be alleviated; therefore, we can compare the performance on a fair basis. We also implement a controller consisting of the linearization torque (4) and the linear control torque (13) in order to demonstrate the effectiveness of the nonlinear control torque (19).

The computed torque plus PID controller has the following form:

$$\boldsymbol{\tau}_{\text{PID}} = \mathbf{M}^*(\mathbf{q})[\ddot{\mathbf{q}}_d + \mathbf{K}_v\dot{\tilde{\mathbf{q}}} + \mathbf{K}_p\tilde{\mathbf{q}} + \mathbf{K}_I\int\tilde{\mathbf{q}}dt] + \mathbf{C}^*(\mathbf{q},\dot{\mathbf{q}})\dot{\mathbf{q}} + \mathbf{G}^*(\mathbf{q}) + \mathbf{B}^*\dot{\mathbf{q}} + \mathbf{F}^*(\dot{\mathbf{q}}) \quad (26)$$

Because there is no velocity feedback, the joint velocity term in $\boldsymbol{\tau}_{\text{PID}}$ is replaced by the backward difference of the joint position. After an extensive manual tuning process, we found that the following PID gains achieve the best tracking performance (in terms of root mean squared errors):

$$\mathbf{K}_p = \text{diag}(800, 500), \quad \mathbf{K}_v = \text{diag}(30, 15), \quad \mathbf{K}_I = \text{diag}(1.411, 0.3)$$

The second controller is $\boldsymbol{\tau}_{\text{Lin}} + \boldsymbol{\tau}_{\text{LC}}$. The design parameters are chosen to be

$$\mathbf{Q}_1 = \text{diag}(32{,}000, 12{,}000, 10, 10), \quad \mathbf{Q}_2 = \text{diag}(0.001, 0.001),$$
$$\mathbf{R} = \text{diag}(0.0005, 0.0015), \quad \lambda_1 = \lambda_2 = 10$$

According to Sec. 3.2, $\mathbf{Q}_1$ emphasizes the performance of the position tracking errors while $\mathbf{Q}_2$ puts smaller weightings on the linear control torque. Here, λ_1 and λ_2 are also weightings for the linear control torque, however, we choose a tiny $\mathbf{R}$ to diminish their effects. In the preceding equation, $\mathbf{R}$ also serves as the weighting of the 1st derivative of the linear control torque.

The last controller is Eq. (3). The following parameters are used for the nonlinear control torque (19):

$$\alpha^* = 4, \quad K_\alpha = 20, \quad \mathbf{A}_\varsigma = \text{diag}(-10, -10),$$
$$\mathbf{B}_\varsigma = \text{diag}(10, 10), \quad \mathbf{C}_\varsigma = \mathbf{I}, \quad G(s) = \frac{100}{s + 100}$$

In other words, the SPR system $\mathbf{H}(s)$ is chosen to be $\text{diag}(10/(s+10), 10/(s+10))$. The selection of $\mathbf{H}(s)$, α,* and K_α follows the rules mentioned in Sec. 3.3.1, while the constraints on $G(s)$ have been discussed in Sec. 3.4.

The experimental results are shown in Figs. 4 and 5. Figures 4(*a*) and 4(*b*) give the trajectories. The corresponding armature voltages of each joint are presented in Figs. 4(*c*) and 4(*d*). Figures 5(*a*) and 5(*b*) show the tracking errors of both joints. A close-up of a 4 s period is given in Figs. 5(*c*) and 5(*d*).

Because the behavior of the friction is more complicated [47] than can be predicted by the simple friction model in Eq. (1), the tracking errors do not converge to zero. Besides, the model parameters θ_i's estimated from experimental data are inaccurate. Nevertheless, the proposed controller (3) has the best performance (in the sense of RMS errors) among all of the controllers tested in this paper. Its superiority is more evident for the 2nd joint. This is because the model parameters of the 2nd joint are less accurate and the controller (3) is the most robust. Note that all controllers exert a similar amount of control inputs, which means that the nonlinear control torque (19) works efficiently. Because of the model uncertainties, the residual $\boldsymbol{\tau}_{\text{Lin}} - \mathbf{h} + \Delta\boldsymbol{\tau}_d$ is not negligible and makes the performance of the 2nd controller less satisfactory;

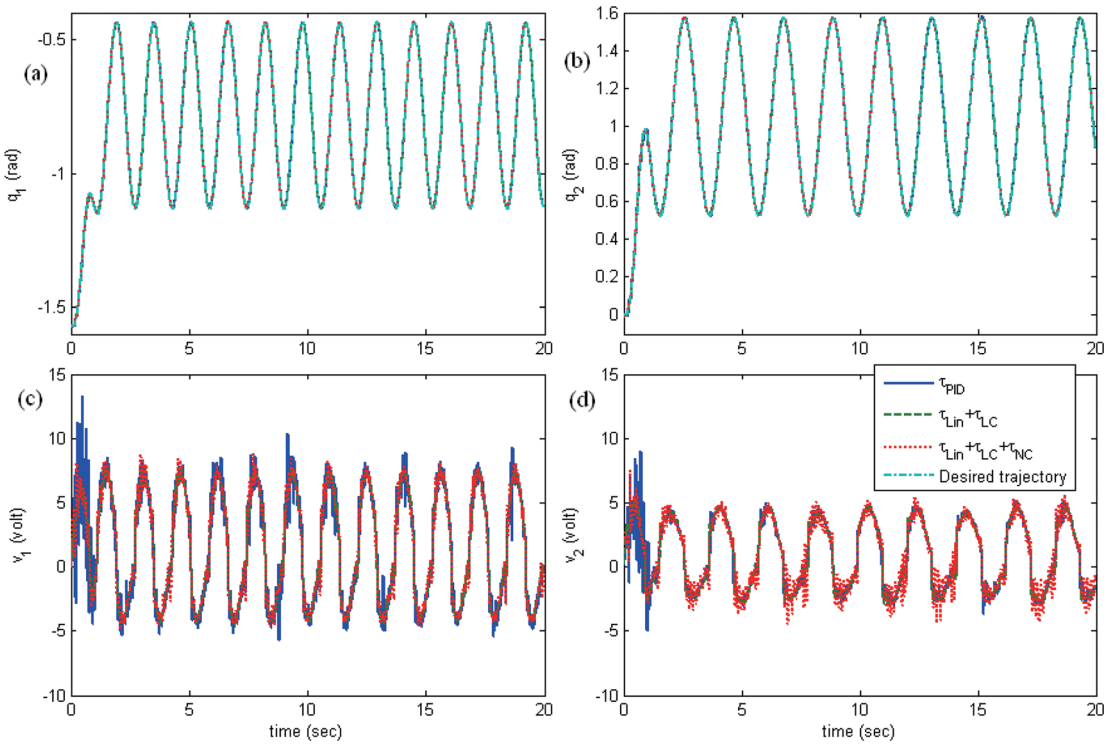

Fig. 4 Experimental results. Solid line (—): τ_{PID}; dashed line (- - -): $\tau_{Lin} + \tau_{LC}$; dotted line (.): $\tau_{Lin} + \tau_{LC} + \tau_{NC}$; dash-dotted line (- · -): desired trajectory. (*a*), (*b*) Positions of the 1st and 2nd joints. (*c*), (*d*) Armature voltages of the 1st and 2nd joints.

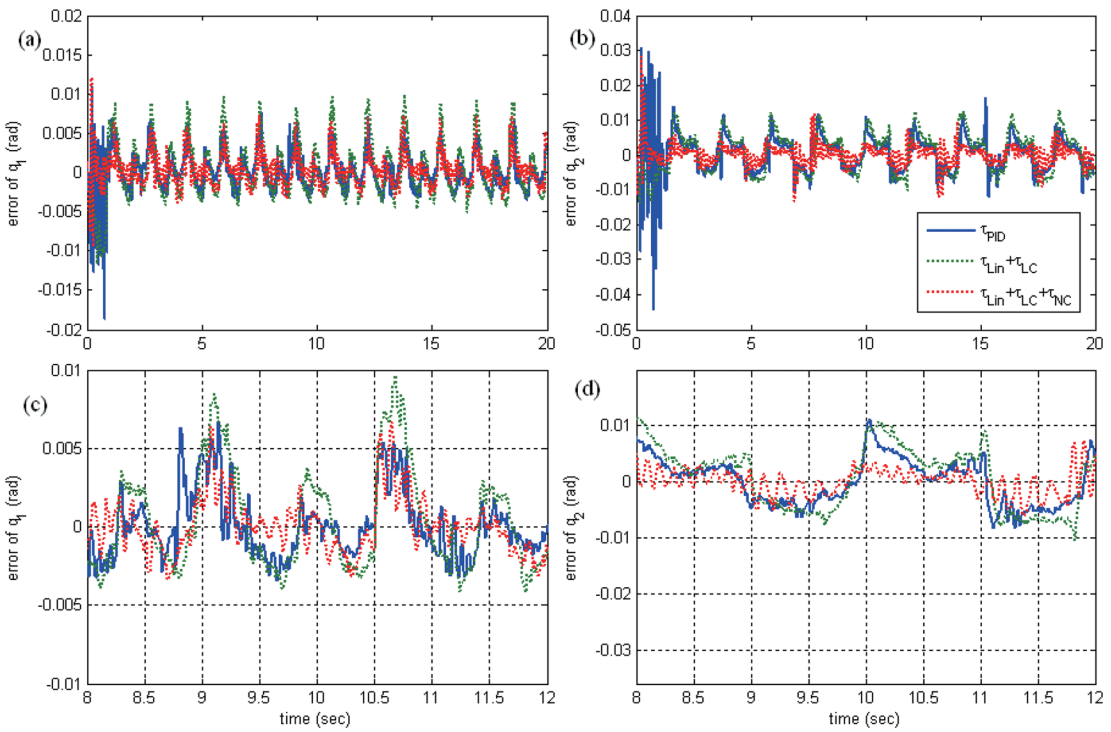

Fig. 5 Position tracking errors. Solid line (—): τ_{PID}; dashed line (- - -): $\tau_{Lin} + \tau_{LC}$; dotted line (· · ·): $\tau_{Lin} + \tau_{LC} + \tau_{NC}$; (*a*) 1st joint: $t = 0$–20 s, (*b*) 2nd joint: $t = 0$–20 s, (*c*) 1st joint: $t = 8$–12 s, and (*d*) 2nd joint: $t = 8$–12 s.

Table 3 Summary of the experimental results

	RMS($\tilde{q}_1$)	RMS($\tilde{q}_2$)	RMS(u_1)	RMS(u_2)
τ_{PID}	0.0026	0.0060	4.6392	2.8659
$\tau_{Lin} + \tau_{LC}$	0.0037	0.0059	4.5017	2.8639
$\tau_{Lin} + \tau_{LC} + \tau_{NC}$	0.0021	0.0032	4.5251	2.8373

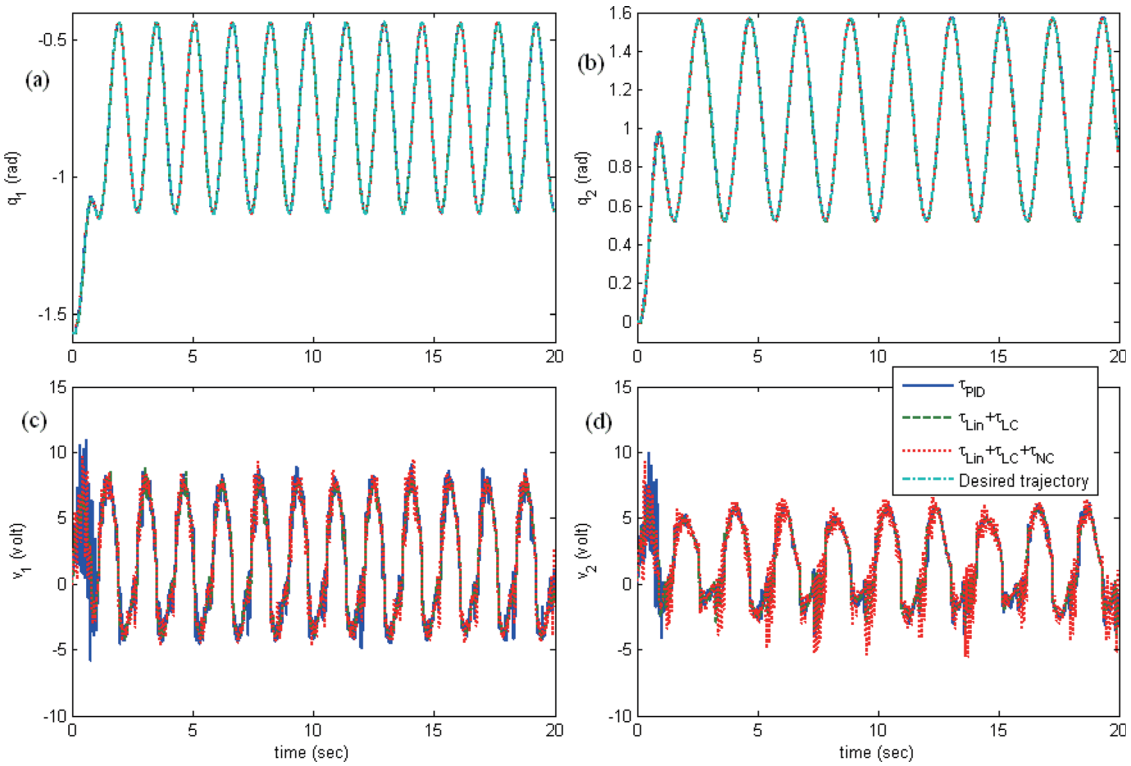

Fig. 6 Experimental results when m_2 increases 33%. Solid line (—): τ_{PID}; dashed line (- - -): $\tau_{Lin}+\tau_{LC}$; dotted line (· · ·): $\tau_{Lin}+\tau_{LC}+\tau_{NC}$; dash dotted line (- · -): desired trajectory. (*a*),(*b*) Positions of the 1st and 2nd joints. (*c*), (*d*) Armature voltages of the 1st and 2nd joints.

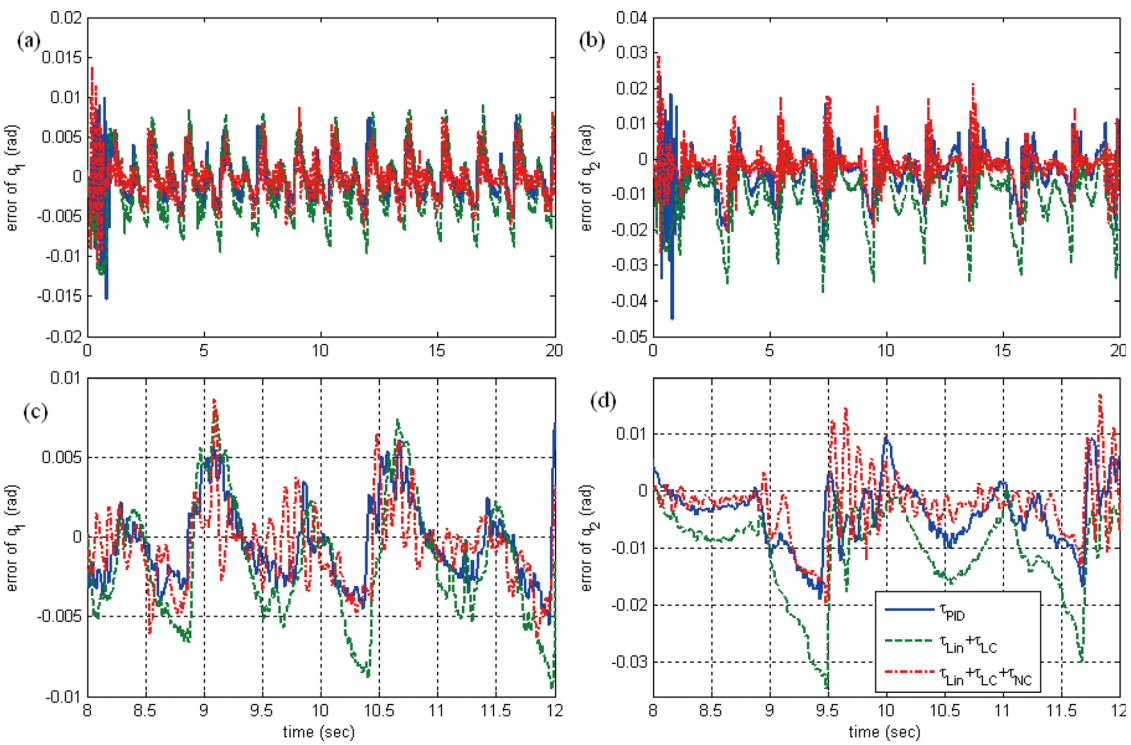

Fig. 7 Position tracking errors when m_2 increases 33%. Solid line (—): τ_{PID}; dashed line (- - -): $\tau_{Lin}+\tau_{LC}$; dotted line (.): $\tau_{Lin}+\tau_{LC}+\tau_{NC}$; (*a*) 1st joint: $t=0$–20 s, (*b*) 2nd joint: $t=0$–20 s, (*c*) 1st joint: $t=8$–12 s, and (*d*) 2nd joint: $t=8$–12 s.

Table 4 Summary of the robustness test

	RMS($\tilde{q}_1$)	RMS($\tilde{q}_2$)	RMS(u_1)	RMS(u_2)
$\boldsymbol{\tau}_{\text{PID}}$	0.0028	0.0076	4.6457	3.3094
$\boldsymbol{\tau}_{\text{Lin}} + \boldsymbol{\tau}_{\text{LC}}$	0.0045	0.0129	4.5621	3.2736
$\boldsymbol{\tau}_{\text{Lin}} + \boldsymbol{\tau}_{\text{LC}} + \boldsymbol{\tau}_{\text{NC}}$	0.0025	0.0058	4.6574	3.4224

however, it is noticeable that the corresponding tracking error is the smoothest. This is because the cost function (16) includes a penalizing term $\dot{\boldsymbol{\eta}}$, which is related to the first derivative of the linear control torque.

Table 3 summarizes the experimental results

$$\text{RMS}(\tilde{q}_1) \triangleq \sqrt{\frac{1}{N_0}\sum_{k=1}^{N_0} |\tilde{q}_1(kT_s)|^2}$$

is the root mean square value of $\tilde{q}_1$, where N_0 is the number of data points. Similar definitions apply to RMS($\tilde{q}_2$), RMS(u_1), and RMS(u_2). Note that the RMS($\tilde{q}_2$) of the proposed controller is only about half of that of the PID controller. This result verifies the effectiveness of the proposed controller.

4.3 Robustness Test. The estimated parameters θ's are uncertain themselves; therefore, the experiment in the previous subsection has already demonstrated the robustness of the tested controllers. In order to further evaluate the robustness of these controllers, we add a payload of 0.288 Kg (about 33% of m_2) to the tip of the 2nd link. Hence, the mass, the moment of inertia, and the position of the center of gravity of the 2nd link change accordingly. The results are exhibited in Figs. 6 and 7. Figures 6(*a*) and 6(*b*) illustrate the trajectories of both joints. Figures 6(*c*) and 6(*d*) are the armature voltages of the 1st and the 2nd joint, respectively. Figure 7 illustrates the position tracking errors of both joints. A clear view of the tracking errors in a 4 s period is given in Figs. 7(*c*) and 7(*d*). The results of the robustness test are summarized in Table 4.

The increase in the payload simultaneously changes $\mathbf{M}_0$, $\mathbf{M}_1(\mathbf{q})$, $\mathbf{C}(\mathbf{q}, \dot{\mathbf{q}})$, and $\mathbf{G}(\mathbf{q})$. Although the linear control torque (13) is robust with respect to variations of $\mathbf{M}_0$, it is not designed to resist changes in $\mathbf{M}_1(\mathbf{q})$, $\mathbf{C}(\mathbf{q}, \dot{\mathbf{q}})$, and $\mathbf{G}(\mathbf{q})$. Moreover, the lack of velocity information results in a severe performance degeneration of the linearization torque (4) whenever the model uncertainties are significant. Therefore, the 2nd controller $\boldsymbol{\tau}_{\text{Lin}} + \boldsymbol{\tau}_{\text{LC}}$ has the largest tracking errors. On the contrary, the proposed controller (3) is able to deal with the model uncertainties with its nonlinear control torque (19). Hence, it has the best performance. Table 4 shows that the RMS($\tilde{q}_2$) of the proposed controller is about 3/4 of that of the PID controller while the RMS(u_2) is almost identical. These experimental results indicate that the proposed controller is robust and does outperform the conventional computed torque plus PID controller.

5 Conclusion

In this paper, we proposed a nonlinear motion control law for manipulators. The proposed controller needs only the joint position feedback and incorporates velocity estimators implicitly into the controller. It consists of three terms: a linearization torque to compensate the manipulator's nominal nonlinear dynamics, a linear control torque to stabilize the linear part of the manipulator, and a nonlinear control torque to ensure asymptotic zero tracking errors and to enhance robustness. A theoretical analysis and experiments were carried out. The results showed that the proposed controller outperforms the conventional computed torque plus PID controller.

During the experiments it was found that the achievable tracking errors are limited by the unmodeled friction forces. Therefore, a better compensation for the friction forces, especially at the low-speed range, will be the topic of future research.

References

[1] Abdallah, C., Dawson, D. M., Dorato, P., and Jamshidi, M., 1991, "Survey of Robust Control for Rigid Robots," IEEE Control Syst. Mag., **11**(2), pp. 24–30.
[2] Sage, H. G., Mathelin, M. F. D., and Ostertag, E., 1999, "Robust Control of Robot Manipulators: A Survey," Int. J. Control, **72**(16), pp. 1498–1522.
[3] Kreutz, K., 1989, "On Manipulator Control by Exact Linearization," IEEE Trans. Autom. Control, **34**(7), pp. 763–767.
[4] Islam, S., and Liu, P. X., 2011, "PD Output Feedback Control Design for Industrial Robotic Manipulators," IEEE/ASME Trans. Mechatron., **16**(1), pp. 187–197.
[5] Moosavian, S. A. A., and Papadopoulos, E., 2007, "Modified Transpose Jacobian Control of Robotic Systems," Automatica, **43**(7), pp. 1226–1233.
[6] Bevly, D., Dubowsky, S., and Mavroidis, C., 2000, "A Simplified Cartesian-Computed Torque Controller for Highly Geared Systems and Its Application to an Experimental Climbing Robot," ASME J. Dyn. Sys., Meas., Control, **122**(1), pp. 27–32.
[7] Kelly, R., and Moreno, J., 2005, "Manipulator Motion Control in Operational Space Using Joint Velocity Inner Loops," Automatica, **41**(8), pp. 1423–1432.
[8] Spong, M. W., 1992, "On the Robust Control of Robot Manipulators," IEEE Trans. Autom. Control, **37**(11), pp. 1782–1786.
[9] Qu, Z., 1992, "Robust Control of a Class of Nonlinear Uncertain Systems," IEEE Trans. Autom. Control, **37**(9), pp. 1437–1442.
[10] Craig, J. J., Hsu, P., and Sastry, S. S., 1987, "Adaptive Control of Mechanical Manipulators," Int. J. Robot. Res., **6**(2), pp. 16–28.
[11] Ortega, R., and Spong, M. W., 1989, "Adaptive Motion Control of Rigid Robots: A Tutorial," Automatica, **25**(6), pp. 877–888.
[12] Spong, M. W., and Ortega, R., 1990, "On Adaptive Inverse Dynamics Control of Rigid Robots," IEEE Trans. Autom. Control, **35**(1), pp. 92–93.
[13] Slotine, J.-J. E., and Li, W., 1988, "Adaptive Manipulator Control: A Case Study," IEEE Trans. Autom. Control, **33**(11), pp. 995–1003.
[14] Slotine, J.-J. E., and Li, W., 1987, "On the Adaptive Control of Robot Manipulators," Int. J. Robot. Res., **6**(3), pp. 49–59.
[15] Chiu, C.-S., Lian, K.-Y., and Wu, T.-C., 2004, "Robust Adaptive Motion/Force Tracking Control Design for Uncertain Constrained Robot Manipulators," Automatica, **40**(12), pp. 2111–2119.
[16] Slotine, J. J. E., and Sastry, S. S., 1983, "Tracking Control of Non-Linear Systems Using Sliding Surfaces With Application to Robot Manipulators," Int. J. Control, **38**(2), pp. 465–492.
[17] Yeung, K. S., and Chen, Y. P., 1988, "A New Controller Design for Manipulators Using the Theory of Variable Structure Systems," IEEE Trans. Autom. Control, **33**(2), pp. 200–206.
[18] Chen, Y.-F., Mita, T., and Wakui, S., 1990, "A New and Simple Algorithm for Sliding Mode Trajectory Control of the Robot Arm," IEEE Trans. Autom. Control, **35**(7), pp. 828–829.
[19] Zhihong, M., Paplinski, A. P., and Wu, H. R., 1994, "A Robust MIMO Terminal Sliding Mode Control Scheme for Rigid Robotic Manipulators," IEEE Trans. Autom. Control, **39**(12), pp. 2464–2469.
[20] Moura, J. T., Roy, R. G., and Olgac, N., 1997, "Frequency-Shaped Sliding Modes: Analysis and Experiments," IEEE Trans. Control Syst. Technol., **5**(4), pp. 394–401.
[21] Yu, W.-S., and Chen, Y.-H., 2005, "Decoupled Variable Structure Control Design for Trajectory Tracking on Mechatronic Arms," IEEE Trans. Control Syst. Technol., **13**(5), pp. 798–806.
[22] Kelly, R., 1993, "A Simple Set-Point Robot Controller by Using Only Position Measurements," IFAC 12th Triennial World Congress, Sydney, Australia, pp. 527–530.
[23] Berghuis, H., and Nijmeijer, H., 1993, "Global Regulation of Robots Using Only Position Measurements," Syst. Control Lett., **21**(4), pp. 289–293.
[24] Tayebi, A., and Islam, S., 2006, "Adaptive Iterative Learning Control for Robot Manipulators: Experimental Results," Control Eng. Pract., **14**(7), pp. 843–851.
[25] Namvar, M., 2009, "A Class of Globally Convergent Velocity Observers for Robotic Manipulators," IEEE Trans. Autom. Control, **54**(8), pp. 1956–1961.
[26] Jeon, S., Tomizuka, M., and Katou, T., 2009, "Kinematic Kalman Filter (KKF) for Robot End-Effector Sensing," ASME J. Dyn. Sys., Meas., Control, **131**(2), p. 021010.
[27] Zhu, W.-H., and Lamarche, T., 2007, "Velocity Estimation by Using Position and Acceleration Sensors," IEEE Trans. Ind. Electron., **54**(5), pp. 2706–2715.
[28] Su, Y. X., Zheng, C. H., Mueller, P. C., and Duan, B. Y., 2006, "A Simple Improved Velocity Estimation for Low-Speed Regions Based on Position Measurements Only," IEEE Trans. Control Syst. Technol., **14**(5), pp. 937–942.
[29] Wit, C. C. D., and Fixot, N., 1991, "Robot Control via Robust Estimated State Feedback," IEEE Trans. Autom. Control, **36**(12), pp. 1497–1501.
[30] Martinez-Guerra, R., Poznyak, A., Gortcheva, E., and Leon, V. D. D., 2000, "Robot Angular Link Velocity Estimation in the Presence of High-Level Mixed Uncertainties," IEEE Proc.: Control Theory Appl., **147**(5), pp. 515–522.
[31] Arteaga, M. A., 2003, "Robot Control and Parameter Estimation With Only Joint Position Measurements," Automatica, **39**(1), pp. 67–73.
[32] Kaneko, K., and Horowitz, R., 1997, "Repetitive and Adaptive Control of Robot Manipulators With Velocity Estimation," IEEE Trans. Robot. Autom., **13**(2), pp. 204–217.
[33] Zhu, W.-H., Chen, H.-T., and Zhang, Z.-J., 1992, "A Variable Structure Robot Control Algorithm With an Observer," IEEE Trans. Robot. Autom., **8**(4), pp. 486–492.

[34] Kelly, R., Santibanez, V., and Loria, A., 2005, *Control of Robot Manipulators in Joint Space*, Springer, New York.
[35] Doyle, J. C., Glover, K., Khargonekar, P. P., and Francis, B. A., 1989, "State-Space Solutions to Standard H_2 and H_∞ Control Problems," IEEE Trans. Autom. Control, **34**(8), pp. 831–847.
[36] Yuz, J. I., and Salgado, M. E., 2003, "From Classical to State-Feedback-Based Controllers," IEEE Control Syst. Mag., **23**(4), pp. 58–67.
[37] Khargonekar, P. P., Petersen, I. R., and Rotea, M. A., 1988, "H_∞-Optimal Control With State-Feedback," IEEE Trans. Autom. Control, **33**(8), pp. 786–788.
[38] Doyle, J. C., 1978, "Guaranteed Margins for LQG Regulators," IEEE Trans. Autom. Control, **23**(4), pp. 756–757.
[39] Anderson, B. D. O., and Moore, J. B., 1990, *Optimal Control: Linear Quadratic Methods*, Prentice Hall, Englewood Cliffs, NJ.
[40] Chilali, M., and Gahinet, P., 1996, "H_∞ Design With Pole Placement Constraints: An LMI," IEEE Trans. Autom. Control, **41**(3), pp. 358–367.
[41] Khargonekar, P. P., and Rotea, M. A., 1991, "Mixed H_2/H_∞ Control: A Convex Optimization Approach," IEEE Trans. Autom. Control, **36**(7), pp. 824–837.
[42] Leitmann, G., 1979, "Guaranteed Asymptotic Stability for Some Linear Systems With Bounded Uncertainties," ASME J. Dyn. Sys., Meas., Control, **101**(3), pp. 212–216.
[43] Ioannou, P. A., and Sun, J., 1996, *Robust Adaptive Control*, Prentice-Hall, Englewood Cliffs, NJ.
[44] Franklin, G. F., Powell, J. D., and Workman, M. L., 1990, *Digital Control of Dynamic Systems*, Addison-Wesley, Reading, MA.
[45] Desoer, C. A., and Vidyasagar, M., 1975, *Feedback Systems: Input-Output Properties*, Academic, New York.
[46] Ljung, L., 1999, *System Identification: Theory for the User*, Prentice Hall PTR, Englewood Cliffs, NJ.
[47] Padthe, A. K., Drincic, B., Oh, J., Rizos, D. D., Fassois, S. D., and Bernstein, D. S., 2008, "Duhem Modeling of Friction-Induced Hysteresis," IEEE Control Syst. Mag., **28**(5), pp. 90–107.